Nanoscale

PAPER

View Article Online
View Journal | View Issue

Cite this: *Nanoscale*, 2023, **15**, 5074

Electro- and photoactivation of silver–iron oxide particles as magnetically recyclable catalysts for cross-coupling reactions†

Qi Wang,[a] Zhongxia Shang,[b] Haiyan Wang [b] and Alexander Wei *[a,b]

Received 23rd August 2022,
Accepted 13th February 2023

DOI: 10.1039/d2nr04629f

rsc.li/nanoscale

Colloidal Ag particles decorated with Fe_3O_4 islands can be electrochemically or photochemically activated as inverse catalysts for C(sp^2)–H heteroarylation. The silver–iron oxide (SIO) particles are reduced into redox-active forms by cathodic charging at mild potentials or by short-term light exposure, and can be reused multiple times by magnetic cycling without further activation. A negative shift in the reduction peak is attributed to an overpotential produced by surface Fe_3O_4 which separates residual Ag ions or clusters from bulk silver. The catalytic efficiency of SIO is maintained even with acid degradation, which can be countered simply by adding water to the reaction medium.

Introduction

Electronic interfacial interactions (EII) in binary catalysts have been studied extensively for their impact on heterogeneous catalysis.[1] Optimization of EII can provide enormous increases in reactivity relative to single-component catalysts by tuning composition ratios, adding dopants, or structural reorganization *via* heat, light, or electrochemistry.[2,3] Metal-oxide composites are the most common form of binary catalyst and can be categorized as metal islands on oxide substrates or as oxides on metal substrates (inverse catalysts), whose EII can differ greatly despite having similar interfaces.[1] Interfacial electron transfer (IET) can occur spontaneously when the metal's Fermi energy level (E_F) is above the oxide's conduction band (E_C) or below its valence energy band (E_V); more often, the E_F lies somewhere in between resulting in partial charge transfer (band bending).

Numerous metal–oxide catalysts have been developed for solution-phase oxidation or reduction of functional groups on organic compounds. Examples involving binary catalysts include the chemoselective reduction of nitroarenes[4,5] and unsaturated aldehydes,[6] hydrogenolysis of polyols,[7] allylic and benzylic oxidations,[8] and aerobic oxidation of alcohols.[9] Several involve relatively inexpensive metals such as Ag and Cu, whose work functions are lower than that of Pd, Pt, or Au and which have rather different EII at the metal-oxide interface.[10]

Heterogeneous binary catalysts have also been developed for homo- and cross-coupling reactions, but the great majority of these involve precious metals such as Pd[11–14] or Au.[15,16] Catalysts based on less expensive metals such as Cu or Ag are clearly desirable, but developments thus far involve metal ions or hydroxides on carbon substrates rather than oxides,[17–19,20] and their activities are not derived from EII. Given the diversity of metal-oxide catalysts already developed for functional group transformations, it is remarkable that they remain largely untapped in the development of new catalysts for C–C bond formation.

Opportunities to design heterogeneous catalysts for cross coupling are even more enticing if materials can be recovered magnetically, permitting their reuse for multiple cycles.[21–24] Although the efficient recovery and recycling of catalysts mounted on superparamagnetic iron-oxide particles has been demonstrated many times, the direct involvement of iron oxide in the catalytic cycle is less common.[25–27] With respect to binary metal-oxide catalysts, we note that Ag-coated Fe_2O_3 and Fe_3O_4 particles have been shown to catalyze the reduction of nitroaromatics,[28–30] the epoxidation of styrene,[31] and the photo-degradation of organic dyes.[32,33] Very recently, Ag-coated Fe_3O_4 has been used to catalyze the oxidation and condensation of benzylic alcohols into dihydrochalcones.[57]

Here we describe the synthesis of magnetically responsive silver–iron oxide (SIO) particles and their use as heterogeneous redox catalysts for direct C(sp^2)–H heteroarylation, a frequently used method for the cross coupling of heterocycles and

[a]*Dept. of Chemistry, Purdue University, 560 Oval Drive, West Lafayette, IN, USA. E-mail: alexwei@purdue.edu*
[b]*Dept. of Materials Science and Engineering, Purdue University, 525 Northwestern Ave, West Lafayette, IN, USA*

†Electronic supplementary information (ESI) available: Additional synthesis details and characterization data for SIO and cross-coupling products, and elemental analysis. See DOI: https://doi.org/10.1039/d2nr04629f

aryldiazonium ions in the synthesis of pharmaceutical intermediates.[34,35] These materials differ from previous Ag/Fe_xO_y catalysts in several respects: (i) they are inverse catalysts with iron oxide serving as the minor species; (ii) they are strongly plasmon-resonant, similar to other types of colloidal Ag; and (iii) they can be prepared under green chemistry conditions in aqueous solutions without amphiphilic surfactants. C(sp^2)–H arylation is a valuable benchmark in cross-coupling chemistry and has been used to introduce novel catalytic mechanisms, such photoredox organocatalysis[36] and mechano-redox catalysis using piezoelectric materials.[37] In this paper we show that SIO particles can be activated as cross-coupling catalysts by two different mechanisms, and recycled multiple times with high retention of catalytic activity.

Results and discussion

Synthesis and characterization

Colloidal SIO can be prepared as aqueous suspensions in a scalable fashion, using mild and inexpensive reagents (Scheme 1). Conditions are adopted from earlier procedures used to prepare magnetic gold nanoclusters.[38] In brief, colloidal Fe_3O_4 (prepared in gram quantities by coprecipitation) were conditioned with 5 kDa polyethylene glycol and L-histidine at pH 6, then treated with $AgNO_3$ (Ag : Fe mole ratio = 4 : 1) and sodium ascorbate as a reductant. This simple procedure produces submicron SIO particles (250–600 nm) with nearly quantitative conversion of Ag (Fig. 1); they are superparamagnetic (M_s = 2.3 emu g^{-1}; Fig. S2; ESI†) and can be collected as a yellow-tan solid using a handheld magnet, then resuspended in water or polar organic solvents with a dispersion half-life of several hours. SIO suspensions exhibit broadband absorption across visible and near-infrared wavelengths with a dip at 320 nm, characteristic of localized plasmon resonance produced by colloidal silver.[39] Indeed, analysis by atomic absorption spectroscopy (AAS) revealed SIOs to be >95% silver (Ag : Fe mass ratio *ca.* 25 : 1).

High-resolution transmission electron microscopy (HRTEM) and elemental imaging by energy-dispersive X-ray spectroscopy (EDS) revealed colloidal SIO to exist as a crystalline Ag core studded with islands of iron oxide (Fig. 2), accompanied by small amounts of free oxide (Fig. S1, ESI†).

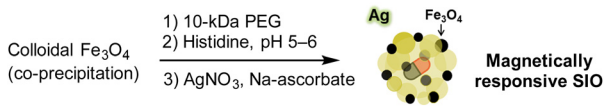

Scheme 1 Aqueous synthesis of colloidal silver–iron oxide (SIO).

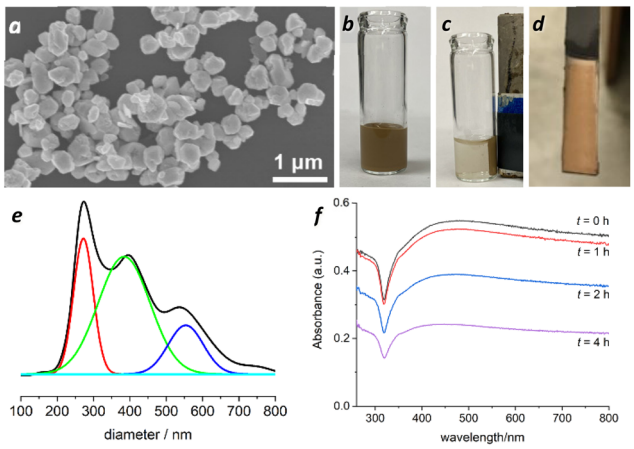

Fig. 1 (a) SEM image of colloidal SIO; (b and c) aqueous dispersion of SIO, before and after collection by NeFeB magnet; (d) colloidal SIO deposited on carbon plate; (e) size distribution of SIO particles by nanoparticle tracking analysis; (f) absorbance spectra of aqueous SIO dispersion (0.1 mg mL^{-1}) with a half-life of several hours.

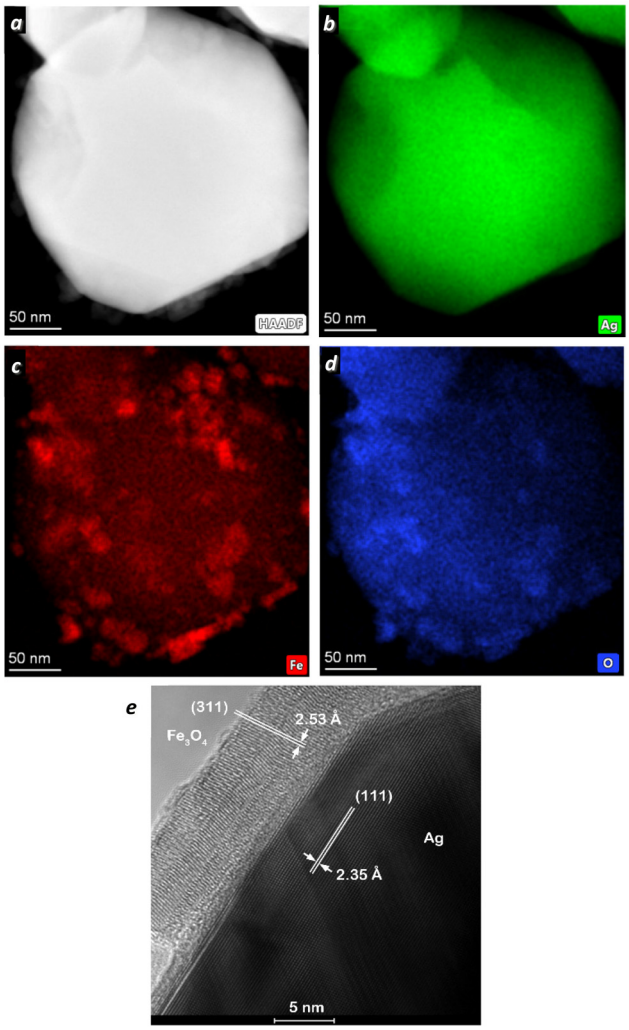

Fig. 2 (a) HAADF-STEM image of SIO; (b–d) EDS images with elemental mapping for Ag ($L\alpha_1$: 2.9846 keV), Fe ($K\alpha_1$: 6.4031 keV, $K\alpha_2$: 6.3895 keV), and O (Kα: 524 eV); (e) HRTEM image of stratified Fe_3O_4 domains on Ag.

XRD confirmed the fcc-Ag core and XPS established the iron oxide to be Fe_3O_4, based on ratiometric intensity of the Fe 3p peak (Fig. S3 and S4, ESI†).[40] A close inspection of islands suggests these to be stratified layers of crystalline Fe_3O_4 with the [311] direction oriented parallel to the interface. This implies that exposed and terminal Fe_3O_4 surfaces may be defined by orthogonal lattice planes such as [211], however we are unable to confirm if the crystalline Fe_3O_4 facet is in direct contact with the Ag interface or separated by a disordered iron-oxide phase.

Catalytic activation and mechanisms

C(sp^2)–H arylation reactions using aryldiazonium salt **1a** and furan as substrates (Scheme 2) were initially performed with as-prepared SIO, which produced 2-arylfuran **1b** in low yield (3.4%; Table 1). However, yields increased to 70% or higher upon catalyst activation. SIOs could be activated electrochemically at mildly cathodic potentials: colloidal SIO was deposited onto a conductive carbon plate using a magnetic field gradient (Fig. 1d), followed by electrochemical activation at −0.3 V *vs.* Ag/AgCl and dispersion into deaerated solvent. Cathodic charging of colloidal SIO increased its equilibrium zeta potential from −19.6 to −34.3 mV, indicative of electrochemical reduction. We also determined that SIOs could be activated photochemically: exposing reaction mixtures of **1a**, furan, and SIO to a 300 W sunlamp for as little as 5 minutes provided high yields of **2a** (Table 1). In both cases, the mole ratios of Ag and Fe to **1a** were 0.05 and 0.004 respectively, establishing SIO activity to be catalytic in nature.

To confirm whether the catalytic properties of SIO are associated uniquely with its chemical composition, C(sp^2)–H arylations were also performed with colloidal Fe_3O_4, colloidal Ag prepared without Fe_3O_4, and mixtures of the two. Cathodic activation of individual colloidal species resulted in no cross-coupling, whereas activation of colloidal mixtures provided a 1.7% yield. This clearly supports the importance of binary metal-oxide structure and EII in catalytic activity.

The SIOs retain their high catalytic activity after a single activation, whether by electrochemical or photochemical mechanisms. SIOs were harvested with a handheld magnet and separated from the reaction mixture then redispersed in fresh medium, and cycled in this manner multiple times. While some attrition of catalyst may be observed (see below), the reaction yield remains uniformly high even after the fifth cycle (Table 2). Multiple cycles performed with constant light irradiation did not provide significant improvements in yield (Table S1, ESI†).

Cross-coupling reactions with aryldiazonium salts are widely believed to proceed by single-electron reduction into an aryl radical or metal-stabilized species,[41] followed by coupling and back-electron transfer to complete the catalytic cycle (Scheme 2). We reasoned that the cathodic reduction of SIO produces an electroactive species that could participate in redox catalysis. Supporting evidence was obtained by evaluat-

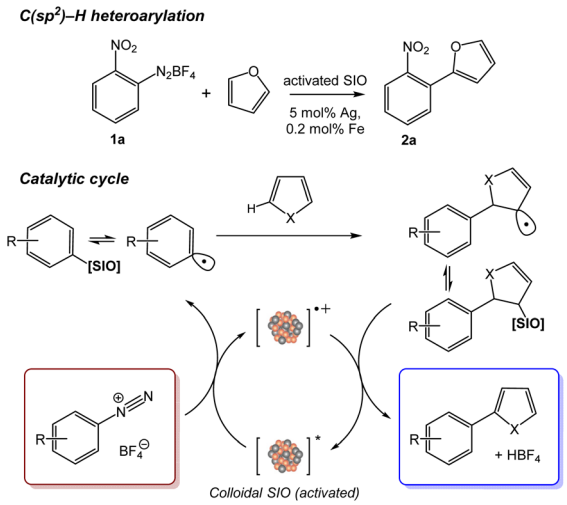

Scheme 2 Direct C–H arylation using furan and activated SIO and presumed catalytic redox cycle.

Table 1 Catalytic activity of SIO and related colloidal species[a]

Catalyst (activation condition)	Yield of **2a** [b] (%)
SIO (no activation)	3.4
SIO (cathodic activation)[c]	72
SIO (photoactivation)[d]	74
Fe_3O_4 only (cathodic)[c]	0
Ag only (cathodic)[c]	0
Fe_3O_4 and Ag (cathodic)[c]	1.7

[a] Standard reaction condition: SIO (3 mg), **1a** (0.5 mmol), furan (5 mmol), DMSO (0.6 mL), 1.5 h, RT. [b] Based on NMR integration (±5%) using CH_2Br_2 as an internal reference. [c] −0.3 V *vs.* Ag/AgCl. [d] Reaction condition: SIO (2 mg), **1a** (0.5 mmol, 1 equiv.), furan (5 mmol), DMSO (0.6 mL), white light (300 W), 5 min, RT.

Table 2 Magnetic recycling of activated SIOs

Reaction conditions	Yield[d] (%)
Cathodic activation[a]	
1st Cycle	69
2nd Cycle	69
3rd Cycle	67
4th Cycle	69
5th Cycle	72
Photoactivation[b]	
1st Cycle[c]	64
2nd Cycle	66
3rd Cycle	67
4th Cycle	63
5th Cycle	60

[a] Standard condition: SIO (15 mg), **1a** (2.5 mmol, 1 equiv.), furan (25 mmol), DMSO (1 mL), 1.5 h, RT. [b] Standard condition: SIO (10 mg), **1a** (2.5 mmol), furan (25 mmol), DMSO (1 mL), 5 min, RT. [c] See Table 1, footnote d. [d] Based on NMR (±5%).

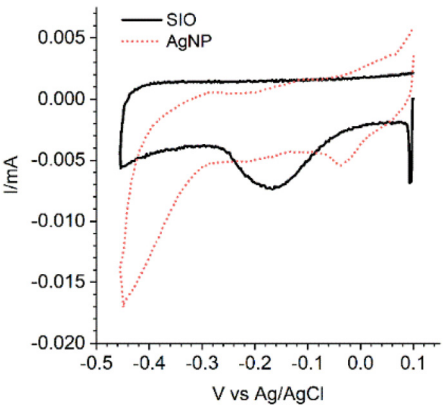

Fig. 3 Cyclic voltammetry of SIO (solid black curve) adsorbed onto glassy carbon (Pt counterelectrode; 15 mM Bu_4NClO_4 in CH_3CN; 10 mV s^{-1} scan rate). Voltammetric scan of colloidal Ag (dotted red curve) included for comparison.

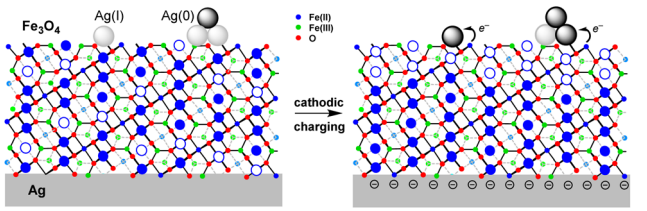

Fig. 4 Cathodic activation of catalytic sites mediated by Fe_3O_4 (interface oriented in [211] direction). Mobile Fe(II) ions (blue) migrate in response to charged Ag interface, resulting in vacancies (white) and negative charge density at the surface, followed by electron transfer from other nearby Fe(II) to Ag(I).

ing the electrochemical activation of SIO by cyclic voltammetry at a slow scan rate. SIOs cast onto a glassy carbon electrode produced an irreversible reduction peak at −0.17 V *vs.* Ag/AgCl (Fig. 3), whereas the half-wave peak produced by colloidal Ag alone was −0.02 V, attributable to the reduction of residual Ag(I). The 150 mV shift in cathodic reduction indicates the role of EII in stabilizing a redox-active species on the SIO surface. This notion is strengthened further by evaluating catalytic activity as a function of cathodic potential: colloidal SIO is fully activated within 15 min when reduced at −0.3 V but less so at milder potentials; however, a longer charging time increases catalytic activity even at −0.1 V (Table 3).

One possible explanation for the 150 mV shift in cathodic reduction is the deposition of residual Ag ions or clusters during SIO synthesis onto Fe_3O_4 islands, which provides physical separation from colloidal Ag (Fig. 4). Fe_3O_4 is a semiconductor that is capable of mediating interfacial electron transfer (IET), but also adds a barrier that can generate an overpotential. Reduction of isolated Ag species produces active sites with low coordination number that can facilitate electron transfer or bonding with aryldiazonium ions (Scheme 2). We note that reactive cluster formation is a commonly cited mechanism for generating strong metal-support interactions (SMSI) that can enhance the activity of binary catalysts.[1–3,42] Analogous forms of this EII have also been described for inverse catalysts, whose oxide layers often exist in high-energy states.[1,43]

The standard reduction potential of bulk Fe_3O_4 is −0.266 V at pH 7 (−0.488 V *vs.* Ag/AgCl),[44] so at first glance IET seems unlikely. However, the Fe(II) ions are highly mobile and can support a redox couple between bulk Ag and isolated catalytic sites. Applying a mild cathodic potential to the SIO creates a buildup of negative charge on the colloidal Ag surface, in response to a net migration of Fe(II) toward the Ag–Fe_3O_4 interface (Fig. 4). Ion depletion at the exposed Fe_3O_4 surface increases negative charge density and lowers its work function,[10] which facilitates IET *via* the oxidation of immobilized Fe(II).[45] The ionic conductivity of Fe_3O_4 may thus be responsible for transducing the electrochemical activation of redox-active surface sites, using colloidal Ag as an electron sink. In this regard, we note that the electrochemical promotion of catalysis (EPOC) also relies on ionically conductive ceramics for the field-driven diffusion of oxygen in the solid state,[46] although this form of electrocatalysis requires a constant applied voltage rather than an activation process.

With regard to SIO photoactivation, such examples are rare although structural changes in heterogeneous photocatalysts have been reported numerous times.[3] Earlier studies involved photoswitchable changes in surface chemistry rather than EII,[47] but more recently it has been shown that UV-induced SMSI can enhance the hydrogenation activity of Pd/TiO_2.[42] Single atoms of Co or Cu anchored on CdS or TiO_2 can also be photoreduced into metastable catalysts for photooxidative couplings[48] or H_2 evolution.[49–51] In the case of SIO, photoactivation of the precatalyst begins with plasmon-enhanced absorption,[39] which provides the energy to drive charge transfer across the Ag–Fe_3O_4 interface. Possible mechanisms for modulating EII include plasmon-amplified electron-hole separation in

Table 3 SIO activity as a function of cathodic potential and charging time[a]

E_{act}[b] (V)	t_{act} (min)	Yield[c] (%)
−0.3	5	47
−0.3	10	58
−0.3	15	72
−0.2	15	62
−0.1	15	23
−0.1	35	37

[a] Standard conditions: SIO (5 mg), **1a** (0.5 mmol), furan (5 mmol), DMSO (0.6 mL), 1.5 h at RT on an orbital shaker. [b] SIO activation on carbon cathode *vs.* Ag/AgCl (15 mM Bu_4NClO_4 in CH_3CN), prior to dispersion in DMSO. [c] Based on NMR (±5%).

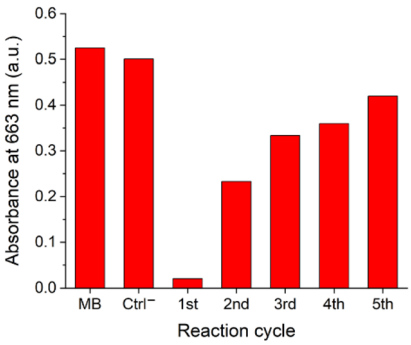

Fig. 5 Reduction of methylene blue (MB, 6 μM) using cathodically activated SIO (−0.3 V *vs.* Ag/AgCl) as a function of reaction cycle; Ctrl$^-$ = unactivated SIO. Increasing retention of absorbance at 663 nm after several cycles indicates SIO functions primarily as a redox catalyst rather than as a reducing agent.

Table 4 Survey of cross-coupling reaction conditions with cathodically activated SIO[a]

SIO (mg mL^{-1})	Furan (equiv.)	Solvent	Yield[b] (%)
5	10	DMSO	70 (isolat.)
3.3			72
1.7			54
5	5	DMSO	62
	2		48
5	10	90% DMSO[c]	64
		CH_3CN	67
		EtOAc	12
		Toluene	2

[a] Standard conditions: 118 mg **1a** (0.5 mmol), 0.36 mL furan, 0.6 mL DMSO, 1.5 h at 25 °C on an orbital shaker. SIO activation performed on carbon cathode (−0.3 V *vs.* Ag/AgCl; 15 mM Bu_4NClO_4 in CH_3CN). [b] Comparison between yields based on NMR integration of **2a**, using CH_2Br_2 as an internal reference. [c] 9 : 1 DMSO : H_2O.

Fe_3O_4 islands followed by interfacial reconstruction,[52] hot-carrier injection for the reduction of catalytic surface sites on Fe_3O_4 (Fig. 4),[53,54] or structurally induced SMSI through a photothermal process.[3]

SIO activation by cathodic charging raises questions whether indirect electrochemical reduction might be involved. In addition, Ag and Fe_3O_4 both have mild reducing power, although control studies confirmed the absence of redox activity even with cathodic charging (Table 1). These issues were addressed by testing the reducing power of SIO with methylene blue (MB), a commonly used redox indicator dye.[55] SIOs were dispersed in an aqueous MB solution adjusted to pH 4.5 (E_{red} = −0.15 V *vs.* Ag/AgCl), then recovered with a magnet and subjected to four more cycles (Fig. 5). A large excess of activated SIO (10 mg) was required to achieve >95% reduction of MB (0.03 μmol) in the initial reaction, as determined by the loss of absorption at 663 nm, whereas unactivated SIO had minimal effect. Subsequent cycles with recovered SIO indicated an attenuation in reducing efficiency. In comparison, reaction yields for cross-coupling remained essentially constant over five reaction cycles (Table 2), confirming their activity as redox catalysts. We also performed cross coupling with SIO exposed to 5 treatments of MB and obtained the desired product in 71% yield. Thus, while activated SIO particles are capable of indirect electrochemical reduction of MB, they are not stoichiometric reducing agents.

Scope and limitations of SIO-catalyzed cross couplings

The reaction conditions for SIO activation and cross coupling are remarkably flexible. Optimum activity is achieved within 5 minutes of light exposure at 300 W or 15 minutes of charging at −0.3 V (Table 2), however lower cathodic potentials can also be used, showing that the catalytic species within SIO can be generated at very low open-circuit potentials (Table 3). Reaction conditions were also surveyed as a function of SIO loading, furan equivalents, and solvent (Table 4). We note that SIO-catalyzed C–H heteroarylation works best in polar aprotic media with DMSO being the optimal solvent, but can also proceed efficiently in the presence of water.

The scope of SIO-catalysed coupling was investigated using various aryldiazonium salts and aromatic heterocycles as substrates for C(sp^2)–H arylation (Table 5). These yields are similar to those reported for redox-catalysed couplings mediated by Cu(I) salts[56] or the mechanochemical activation of colloidal $BaTiO_3$.[7] The presence of halogen substituents (Cl, Br, and I) on acceptors **1b–1e** does not interfere with C(sp^2)–H arylation, despite the presence of silver. However, *para*-substituted acceptors **1f–1h** and *ortho*-carboethoxy derivative **1i** produce furylated products in lower yields relative to **1b–1e**, suggesting that the *ortho*-nitro group helped to stabilize the reactive intermediate. Activated SIO could also mediate the coupling of **1a** with other heteroaromatics to produce heterobiaryl species **3a–5a**. The magnetic SIO catalysts are so far unique in their capacity for recovery and reuse over multiple reaction cycles, and their compositions may be tuned for further improvements in catalytic efficiency.

While the highest reaction yields can be achieved with an initial SIO loading of 3.3 mg mL^{-1} (Table 4), subsequent reactions with recycled catalyst indicate that the amount needed to support efficient conversion is in fact much lower. This was determined by using AAS to quantify the amounts of Ag and Fe in magnetically recovered SIO and non-magnetic solute following each reaction cycle (Tables 6, S2, and S3, ESI†). Under standard conditions, the mass recovery of magnetic SIO after five consecutive reactions was 23% with significant amounts of non-magnetic solute generated in between recovery cycles, yet despite this degradation the reaction yields remained at or above 70% (Table 2). We note that the non-magnetic residue also consisted of Ag nanoparticles loosely attached

Table 5 Survey of substrates for C–H heteroarylation[a]

Aryl acceptor		Heteroarene	Product		Yield[b]
1a	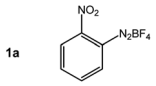	Furan	**2a**	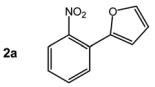	70(72)
1b	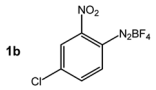	Furan	**2b**	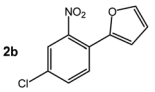	(72)
1c	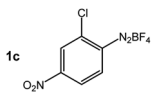	Furan	**2c**	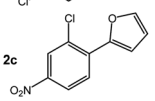	60(65)
1d	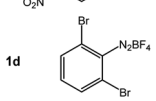	Furan	**2d**	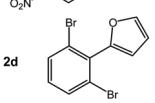	(72)
1e	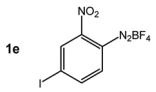	Furan	**2e**	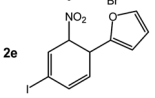	(74)
1f	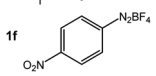	Furan	**2f**	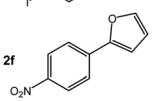	53(60)
1g	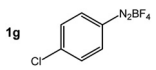	Furan	**2g**	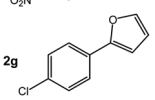	(46)
1h	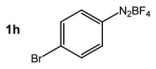	Furan	**2h**	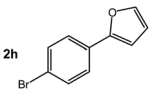	(57)
1i	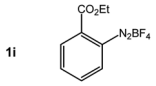	Furan	**2i**	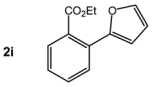	(42)
1a	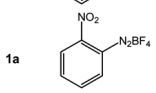	Thiophene	**3a**	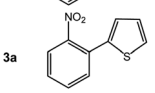	57[c]
1a	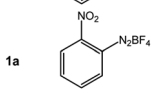	Benzofuran	**4a**	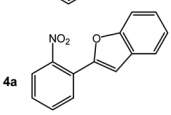	35
1a	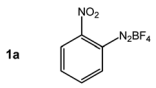	*N*-boc-pyrrole	**5a**	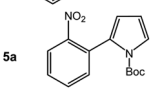	67

[a] Standard conditions: 0.5 mmol arenediazonium salt, 10 equiv. heteroarene, 3 mg activated SIO, 0.6 mL DMSO, 1.5 h at 25 °C on an orbital shaker. [b] Isolated yields (NMR yields in parentheses). [c] 93 : 7 Mixture of isomers (major shown).

to iron oxide (Fig. S5, see ESI†), but lacked catalytic activity.

The primary cause for SIO degradation is HBF_4, a byproduct of C–H heteroarylation (Scheme 2). We thus performed reactions with base to determine the effect of neutralization on SIO preservation and reaction yield. Adding one equiv. of Et_3N enabled a mass recovery of magnetic SIO above 90% after 5 cycles, with residual iron oxide from SIO synthesis accounting for nearly all of the loss (Table 6); however, the reaction yield was reduced to 40% per cycle. After testing several weaker bases, we found 10% water in DMSO was sufficient to prevent acid degradation of SIO with 60% mass recovery after 5 reaction cycles, while maintaining an average yield of 60% (Table S 4, ESI†).

Table 6 Elemental analysis of recovered SIO catalyst and mass loss, by AAS[a]

	SIO[b] (standard)		Mass loss[c]		SIO[d] (with base)	
Sample	Ag (ppm)	Fe (ppm)	Ag (ppm)	Fe (ppm)	Ag (ppm)	Fe (ppm)
Before rxn	12 700	500	—	—	9040	580
1st Cycle	—	—	1525	45	—	—
2nd Cycle	—	—	1545	40	—	—
3rd Cycle	—	—	1700	45	—	—
4th Cycle	—	—	1665	40	—	—
5th Cycle	2800	200	1305	30	8880	60

[a] All samples were diluted with water for analysis; values represent total moles. [b] Activated SIO was dispersed in 1 mL DMSO and subjected to standard reaction conditions (Table 3). [c] Non-magnetic solute. [d] Activated SIO subjected to standard conditions plus 1 equiv. Et_3N.

Conclusions

Our studies with colloidal SIO illustrate how metal-oxide particles can be developed as magnetically recyclable redox catalysts for cross-coupling reactions, using less expensive materials such as Ag and Fe_3O_4. In the course of this work, we have identified both electrochemical and photochemical conditions for catalyst activation and propose working mechanisms for each. SIO synthesis and activation conditions are very mild and can catalyze the cross coupling of a broad range of substrates. The growing knowledge base of EII provides ample opportunities to design new binary catalysts for organic synthesis using earth-abundant materials.

Experimental

Synthesis of SIO

Colloidal Fe_3O_4 was prepared by the co-precipitation method then conditioned by sequential treatment with polyethylene glycol (PEG) and L-histidine, as previously described (see ESI for full details†).[38] A solution of $AgNO_3$ (135 mg, 0.795 mmol) was dissolved in 36 mL of deionized water then combined with 63 mL of conditioned Fe_3O_4 (15 mg, 0.194 mmol Fe) and blended for 20 min using an overhead mechanical stirrer. The reaction mixture was treated with 30 mL of 0.08 M sodium ascorbate added by syringe pump over a period of 6 h, which caused the reaction color to change gradually from dark brown to tan. The reaction mixture was allowed to sit for another 6 h to ensure complete formation of colloidal SIO, which was collected over a 15 min period using a handheld NdFeB magnet (local field gradient of 1–3 kG cm^{-1}). After the supernatant and non-magnetic solutes were decanted, the colloidal SIO was subjected to two rounds of redispersion into water followed by magnetic precipitation to yield SIO particles that were essentially devoid of non-magnetic silver. The final mass and composition of SIO was determined to be 90 mg with a Ag : Fe mass ratio of 25 : 1.

Electrochemical SIO activation

A suspension of colloidal SIO (3 mg dry weight) was deposited dropwise onto a conductive carbon plate supported on a NdFeB magnet. After the supernatant was drained, the coated carbon cathode was immersed carefully in a deaerated 15 mM solution of Bu_4NClO_4 in acetonitrile, with the NdFeB magnet propped against the glass wall to prevent redispersion of colloidal SIO. Cathodic charging was performed for 15 min at −0.3 V *vs.* Ag/AgCl using Pt wire as counterelectrode. The SIO particles were dispersed immediately after activation into the deaerated reaction mixture by immersion for several seconds in an ultrasonic bath.

SIO-mediated cross-couplings

Aryldiazonium BF_4 salts were prepared in advance and dried under reduced pressure (see ESI†). Furan was distilled from CaH_2 and reagent-grade solvents were used without further purification. Reaction mixtures were deaerated with argon for five minutes prior to addition of SIO.

Cross coupling with electrochemically activated SIO. In a typical experiment, 3 mg of freshly activated SIO was dispersed into a 3 mL spin vane containing DMSO (0.6 mL), followed by addition of furan (0.36 mL, 10 equiv.) and aryldiazonium salt (118 mg, 0.5 mmol). The reaction vessel was sealed under Ar then agitated on a vortex mixer at rt for 1.5 h, although reaction times as short as 5 minutes could be used (see below). The reaction mixture was decanted from the SIO, which was held in place by an external magnet and rinsed with a few drops of DMSO. The SIO could be reused simply by adding freshly deaerated DMSO, followed by furan and aryldiazonium salt.

Cross coupling with photoactivated SIO. 2 mg of SIO was dispersed into a 3 mL vial containing DMSO (0.6 mL) followed by addition of furan (0.36 mL, 10 equiv.) and aryldiazonium salt (118 mg, 0.5 mmol). The reaction vessel was sealed under Ar then agitated on a vortex mixer at rt for 5 minutes with exposure to a 300 W sunlamp. The SIOs were then removed by magnetic precipitation as described above. All subsequent reactions were performed under ambient lighting.

Product analysis. Reaction mixtures were diluted with 10 mL of deionized water then extracted with ethyl ether (100 mL) and washed with brine solution (100 mL). Isolated yields were obtained by purifying the reaction product by silica gel chromatography (5% Et_2O in pentane or 5% EtOAc in hexanes, depending on product volatility). NMR yields were obtained by dissolving the crude reaction mixture in $CDCl_3$ and adding 30 μL CH_2Br_2 (0.43 mmol; δ 4.92) as internal reference. Spectra were obtained using a 400 MHz NMR spectrometer (Bruker BioSpin).

Atomic absorption spectroscopy (AAS) analysis

The Ag and Fe content of SIO suspensions were determined using a PerkinElmer 3110 spectrometer equipped with UV cathode lamps emitting at 248 nm (Fe) or 328 nm (Ag). Atomic standards for Ag and Fe (1000 ppm each) were prepared respectively by dissolving 7.9 mg $AgNO_3$ and 17.8 mg $FeCl_2{\cdot}4H_2O$ in 5 mL water, then diluted serially with deionized water to generate standard curves between 2.0 and 10.0 ppm. SIO suspensions in 1 mL DMSO were diluted 1200-fold with deionized water for Ag analysis and 160-fold for Fe analysis. Supernatants separated from SIO were first centrifuged at high speed to precipitate non-magnetic solids, then analyzed after 300-fold dilution with DMSO for Ag analysis and after sixfold dilution for Fe analysis. Non-magnetic precipitate was resuspended in 4 mL deionized water for Fe analysis.

Author contributions

Q. W. performed all syntheses and chemical characterizations. S. Z. and H. W. performed electron

microscopy and analysis. Q. W. and A. W. designed the research studies and wrote the manuscript.

Conflicts of interest

There are no conflicts to declare.

Acknowledgements

We gratefully acknowledge financial support from the U.S. National Science Foundation (CHE-2204206, DMR-2016453) and the National Institutes of Health (R01 NS117701, P30 CA023168), Paul Bower for assistance with atomic absorption spectroscopy, Nancy Fu for assistance with APCI-MS characterization, and Jiawei Song for magnetic characterization.

References

1 Y. Li, Y. Zhang, K. Qian and W. Huang, *ACS Catal.*, 2022, **12**, 1268–1287.
2 G.-M. Schwab, in *Advances in Catalysis*, ed. D. D. Eley, H. Pines and P. B. Weisz, Academic Press, 1979, vol. 27, pp. 1–22.
3 L. Liu and A. Corma, *Nat. Rev. Chem.*, 2021, **5**, 256–276.
4 A. Corma and P. Serna, *Science*, 2006, **313**, 332–334.
5 T. Mitsudome, Y. Mikami, M. Matoba, T. Mizugaki, K. Jitsukawa and K. Kaneda, *Angew. Chem., Int. Ed.*, 2012, **51**, 136–139.
6 T. Mitsudome, M. Matoba, T. Mizugaki, K. Jitsukawa and K. Kaneda, *Chem. – Eur. J.*, 2013, **19**, 5255–5258.
7 S. S. Priya, P. Bhanuchander, V. P. Kumar, S. K. Bhargava and K. V. R. Chary, *Ind. Eng. Chem. Res.*, 2016, **55**, 4461–4472.
8 C. D. Pina, E. Falletta and M. Rossi, in *Liquid Phase Oxidation via Heterogeneous Catalysis*, 2013, pp. 221–262.
9 (*a*) V. V. Torbina, A. A. Vodyankin, S. Ten, G. V. Mamontov, M. A. Salaev, V. I. Sobolev and O. V. Vodyankina, *Catalysts*, 2018, **8**, 447; (*b*) E. N. Kolobova, A. N. Pestryakov, N. Bogdanchikova and V. Cortés Corberán, *Catal. Today*, 2019, **333**, 81–88.
10 M. T. Greiner, L. Chai, M. G. Helander, W.-M. Tang and Z.-H. Lu, *Adv. Funct. Mater.*, 2012, **22**, 4557–4568.
11 L. Yin and J. Liebscher, *Chem. Rev.*, 2007, **107**, 133–173.
12 Á. Molnár, *Chem. Rev.*, 2011, **111**, 2251–2320.
13 I. Hussain, J. Capricho and M. A. Yawer, *Adv. Synth. Catal.*, 2016, **358**, 3320–3349.
14 P. P. Mpungose, Z. P. Vundla, G. E. M. Maguire and H. B. Friedrich, *Molecules*, 2018, **23**, 1676.
15 Q. Shi, Z. Qin, H. Xu and G. Li, *Nanomaterials*, 2019, **9**, 838.
16 F. Mohammadparast, A. P. Dadgar, R. T. A. Tirumala, S. Mohammad, C. O. Topal, A. K. Kalkan and M. Andiappan, *J. Phys. Chem. C*, 2019, **123**, 11539–11545.
17 B. H. Lipshutz and P. A. Blomgren, *J. Am. Chem. Soc.*, 1999, **121**, 5819–5820.
18 B. H. Lipshutz, B. A. Frieman and A. E. Tomaso Jr., *Angew. Chem., Int. Ed.*, 2006, **45**, 1259–1264.
19 B. H. Lipshutz, D. M. Nihan, E. Vinogradova, B. R. Taft and ŽV. Bošković, *Org. Lett.*, 2008, **10**, 4279–4282.
20 B. R. Buckley, R. Butterworth, S. E. Dann, H. Heaney and E. C. Stubbs, *ACS Catal.*, 2015, **5**, 793–796.
21 B. Karimi, F. Mansouri and H. M. Mirzaei, *ChemCatChem*, 2015, **7**, 1736–1789.
22 R. K. Sharma, S. Dutta, S. Sharma, R. Zboril, R. S. Varma and M. B. Gawande, *Green Chem.*, 2016, **18**, 3184–3209.
23 R. Kore, A. D. Sawant and R. D. Rogers, *ACS Sustainable Chem. Eng.*, 2021, **9**, 8797–8802.
24 H. Veisi, S. Hemmati and P. Safarimehr, *J. Catal.*, 2018, **365**, 204–212.
25 M. M. Mojtahedi, M. Saeed Abaee and T. Alishiri, *Tetrahedron Lett.*, 2009, **50**, 2322–2325.
26 K. Swapna, A. Vijay Kumar, V. Prakash Reddy and K. Rama Rao, *J. Org. Chem.*, 2009, **74**, 7514–7517.
27 T. Zeng, W.-W. Chen, C. M. Cirtiu, A. Moores, G. Song and C.-J. Li, *Green Chem.*, 2010, **12**, 570–573.
28 M. Kaloti, A. Kumar and N. K. Navani, *Green Chem.*, 2015, **17**, 4786–4799.
29 A. K. Patra, N. T. Vo and D. Kim, *Appl. Catal., A*, 2017, **538**, 148–156.
30 S. Chang, C. Liu, Y. Sun, Z. Yan, X. Zhang, X. Hu and H. Zhang, *ACS Appl. Nano Mater.*, 2020, **3**, 2302–2309.
31 D.-H. Zhang, G.-D. Li, J.-X. Li and J.-S. Chen, *Chem. Commun.*, 2008, 3414–3416.
32 (*a*) S. Zhang, F. Ren, W. Wu, J. Zhou, L. Sun, X. Xiao and C. Jiang, *J. Colloid Interface Sci.*, 2014, **427**, 29–34; (*b*) S. A. Sallam, G. M. El-Subruiti and A. S. Eltaweil, *Catal. Lett.*, 2018, **148**, 3701–3714.
33 C. V. Khedkar, N. D. Khupse, B. R. Thombare, P. R. Dusane, G. Lole, R. S. Devan, A. S. Deshpande and S. I. Patil, *Chem. Phys. Lett.*, 2020, **742**, 137131.
34 R. Rossi, M. Lessi, C. Manzini, G. Marianetti and F. Bellina, *Adv. Synth. Catal.*, 2015, **357**, 3777–3814.
35 H. Bonin, M. Sauthier and F.-X. Felpin, *Adv. Synth. Catal.*, 2014, **356**, 645–671.
36 D. P. Hari, P. Schroll and B. König, *J. Am. Chem. Soc.*, 2012, **134**, 2958–2961.
37 K. Kubota, Y. Pang, A. Miura and H. Ito, *Science*, 2019, **366**, 1500–1504.
38 (*a*) N. R. Kadasala and A. Wei, *Nanoscale*, 2015, **7**, 10931–10935; (*b*) N. R. Kadasala, L. Lu, C. Gilpin and A. Wei, *Sci. Technol. Adv. Mater.*, 2017, **18**, 210–218.
39 A. Wei, in *Nanoparticles: Scaffolds and Building Blocks*, ed. V. M. Rotello, Kluwer Academic, New York, 2004, pp. 173–200.
40 T. Yamashita and P. Hayes, *Appl. Surf. Sci.*, 2008, **254**, 2441–2449.
41 C. Galli, *Chem. Rev.*, 1988, **88**, 765–792.
42 H. Chen, Z. Yang, X. Wang, F. Polo-Garzon, P. W. Halstenberg, T. Wang, X. Suo, S.-Z. Yang,

H. M. Meyer, Z. Wu and S. Dai, *J. Am. Chem. Soc.*, 2021, **143**, 8521–8526.
43 J. A. Rodriguez, P. Liu, J. Graciani, S. D. Senanayake, D. C. Grinter, D. Stacchiola, J. Hrbek and J. Fernández-Sanz, *J. Phys. Chem. Lett.*, 2016, **7**, 2627–2639.
44 H. Peng, C. I. Pearce, W. Huang, Z. Zhu, A. T. N'Diaye, K. M. Rosso and J. Liu, *Environ. Sci.: Nano*, 2018, **5**, 1545–1555.
45 C. A. Gorski and M. M. Scherer, in *Aquatic Redox Chemistry*, American Chemical Society, 2011, 1071, ch. 15, pp. 315–343.
46 P. Vernoux, L. Lizarraga, M. N. Tsampas, F. M. Sapountzi, A. De Lucas-Consuegra, J.-L. Valverde, S. Souentie, C. G. Vayenas, D. Tsiplakides, S. Balomenou and E. A. Baranova, *Chem. Rev.*, 2013, **113**, 8192–8260.
47 B. M. Neilson and C. W. Bielawski, *ACS Catal.*, 2013, **3**, 1874–1885.
48 C. Chen, T. Wu, D. Yang, P. Zhang, H. Liu, Y. Yang, G. Yang and B. Han, *Chem. Commun.*, 2018, **54**, 5984–5987.
49 B.-H. Lee, S. Park, M. Kim, A. K. Sinha, S. C. Lee, E. Jung, W. J. Chang, K.-S. Lee, J. H. Kim, S.-P. Cho, H. Kim, K. T. Nam and T. Hyeon, *Nat. Mater.*, 2019, **18**, 620–626.
50 Y. Guo, Y. Yang, X. Yin, J. Liu and W. Que, *Sustainable Energy Fuels*, 2020, **4**, 2559–2568.
51 L. Ma, L. Mei, Y. Gao, N. Zhang, S. Wang, Q. Li, Z.-H. Liu and R. Jiang, *Appl. Mater. Today*, 2022, **27**, 101417.
52 P. Mishra, S. Patnaik and K. Parida, *Catal. Sci. Technol.*, 2019, **9**, 916–941.
53 U. Aslam, V. G. Rao, S. Chavez and S. Linic, *Nat. Catal.*, 2018, **1**, 656–665.
54 Y. Zhang, W. Guo, Y. Zhang and W. D. Wei, *Adv. Mater.*, 2021, **33**, 2006654.
55 O. S. Ksenzhek, S. A. Petrova and M. V. Kolodyazhny, *Bioelectrochem. Bioenerg.*, 1977, **4**, 346–357.
56 N. Obushak, A. Lesyuk, Y. Gorak and V. Matiichuk, *Russ. J. Org. Chem.*, 2009, **45**, 1375–1381.
57 L. Tang, F. Qin, F. Huang, D. Xu, Q. Hu and W. Zhang, *Appl. Organomet. Chem.*, 2022, **36**, e6723.